PCCP

Accepted Manuscript

ROYAL SOCIETY OF CHEMISTRY

www.rsc.org/pccp

Nonsymmetric 9,10-diphenylanthracene-based deep-blue emitters with enhanced charge transport properties

Tomas Serevičius,[a]* Regimantas Komskis,[a] Povilas Adomėnas,[b] Ona Adomėnienė,[b] Vygintas Jankauskas,[c] Alytis Gruodis,[d] Karolis Kazlauskas[a] and Saulius Juršėnas[a]

[a]Institute of Applied Research, Vilnius University, Saulėtekio 9-III, LT-10222 Vilnius, Lithuania
[b]Fine Synthesis Ltd, Kalvarijų g. 201E, LT-03225 Vilnius, Lithuania
[c]Department of Solid State Electronics, Vilnius University, Saulėtekio 9-III, LT-10222 Vilnius, Lithuania
[d]Department of General Physics and Spectroscopy, Vilnius University, Saulėtekio 9-III, LT-10222 Vilnius, Lithuania

Corresponding Author
*Fax: +370 5 2366059. Phone: +370 5 2366028. E-mail: tomas.serevicius@ff.stud.vu.lt.

Abstract

Realization of efficient deep-blue anthracene-based emitters with superior film-forming and charge transport properties is challenging. A series of nonsymmetric 9,10-diphenylanthracenes (DPA) with phenyl and pentyl moieties at the 2nd position and alkyl groups at *para* positions of the 9,10-phenyls were synthesized and investigated. The nonsymmetric substitution at the 2nd position enabled to improve film forming properties as compared to those of the unsubstituted DPA and resulted in glass transition temperatures of up to 92 °C. Small-sized and poorly conjugated substituents allowed to preserve emission in the deep blue range (<450 nm). Substitution at the 2nd position enabled to achieve high fluorescence quantum yields (up to 0.7 in solution, and up to 0.9 in polymer host), although it caused up to 10-fold increase in the intersystem crossing rate as compared to that of the unsubstituted DPA. Further optimization of the film forming properties achieved by varying length of the alkyl groups attached at the 9,10-phenyls enabled to attain very high hole drift mobilities (~$5\cdot10^{-3}$ - $1\cdot10^{-2}$ cm^2/Vs) in the solution-processed amorphous films of the DPA compounds.

Introduction

Anthracene derivatives nowadays are used in a large variety of chemical, photophysical and medical applications. The most important applications encompasses fluorescence probes and chemosensors,[1] anticancer agents,[2] efficient organic scintillators[3] as well as numerous optoelectronic devices including anthracene-based thin-film transistors,[4–6] solar cells,[7,8] and organic light-emitting diodes (OLEDs).[9–15] The liquid anthracenes are believed to be prospective for the future applications such as low-power color-tunable and light upconversion devices.[16-18] Owing to the high stability and high-efficiency deep-blue fluorescence of anthracene compounds they were found to be particularly attractive for OLED applications.[19] Recently, the interest in anthracenes has even more risen because of the demonstration of OLED efficiency boosting capabilities *via* utilization of triplet-triplet annihilation (or triplet fusion)[12,14] and thermally-

activated delayed fluorescence.[15] The later phenomenon enabled to achieve very high external quantum efficiency (16.5%) in anthracene-based OLED.
Generally, the unsubstituted anthracene is of less practical use in optoelectronics as it suffers from low fluorescence quantum yield (30%) in solution and ready crystallization in the films.[1] To overcome these shortcomings structural modifications of anthracene are commonly used. The most popular way to evade high intersystem crossing rate is an introduction of various substituents into the 9th and 10th positions of molecular anthracene. This substitution enhances strength of an allowed optical transition $S_0 \rightarrow S_1$ with the transition dipole moment lying along the short axis of the anthracene molecule.[20,21] A well-known 9,10-diphenylanthracene (DPA) serves as the nice example of such enhancement boosting fluorescence quantum efficiency up to 95%.[22] Although out-of-plane twisted 9,10-phenyl moieties cause only minimal decrease in the emission energy, which is important for preserving emission in the deep-blue range, they are insufficient to prevent crystallization of DPA films. The crystallization is detrimental as it severely limits efficiency of OLED devices.[23] It was demonstrated that film forming properties of DPA can be improved either by introducing more bulky aryl-based substituents at the 9th and 10th positions[9,11] or by incorporating additional moieties at the 2nd and 6th positions.[24,25] Unfortunately, most of the DPA derivatives subjected to such modifications and exhibiting glassy state showed poor hole drift mobility (μ_h), in the order of 10^{-7} cm/Vs.[26–27] Nevertheless, observations of remarkably higher μ_h for a few DPA derivatives were also reported.[28] For instance, DPA functionalized with arylamino[29] or pyridine[30] moieties resulted in carrier drift mobilities exceeding 10^{-3} cm^2/Vs. However, the downside of the bulky aromatic substituents was extension of π-conjugated electron system, which shifted compound emission to longer wavelengths (>450 nm). Therefore, one of the challenges from the optoelectronic application point of view could be the realization of anthracene-based deep-blue emitters featuring fluorescence efficiencies close to DPA, though, in the contrast to DPA, demonstrating good film forming properties and high carrier drift mobilities. Excellent emission and charge transport properties realized in the same functional layer accompanied with solution processability could make the anthracene emitters promising for simplified architecture deep-blue OLEDs.
To this end, a series of structurally modified nonsymmetric 9,10-diphenylanthracene derivatives (Figure 1) were synthesized and investigated. To enhance film forming properties of the DPA derivatives they were nonsymmetrically substituted at the 2nd position by using either phenyl or pentyl moiety. The impact of different length alkyl groups attached at the *para* position of 9,10-phenyls on the fluorescence efficiency, concentration quenching and carrier drift mobility was also studied. The influence of various substituents on the electron density distribution in molecular orbitals, energy spectrum of singlet and triplet manifolds, and oscillator strengths of the studied DPA derivatives was evaluated by density functional theory calculations, which were compared with experimental data.

Experimental methods

Instrumentation.

H1, C13 NMR spectra were measured using BRUKER ASCEND 400 (400 MHz) and Varian Unity Inova 300 (300 MHz) spectrometers. Purity of synthesized materials was analyzed using Agilent Technologies 6890N Network GC System and Agilent Technologies 7890C GC systems gas chromatographs. Mass spectra were set using Agilent Technologies 5975C gas

chromatograph/mass selective detector (GC/ MSD) system with the triple-axis detector. HRMS mass spectrometry analyses were carried out on a quadrupole, time-of-flight mass spectrometer (micrOTOF-Q II, Bruker Daltonik GmbH). Melting points of the materials were determined using Thermo Scientific 9100 apparatus. Differential scanning calorimetry (DSC) measurements were carried out using DSC 8500 (PerkineElmer) thermal analysis system at a heating/cooling rate of 10 °C/min under nitrogen flow. Optical properties of the DPA derivatives were assessed in dilute 10^{-6} M tetrahydrofuran (THF) solutions and wet-casted films prepared from 5×10^{-3} M THF solutions. Absorption spectra were recorded on a UV−Vis−NIR spectrophotometer Lambda 950 (Perkin-Elmer). Fluorescence of the investigated compounds was excited by a 365 nm wavelength light from Xe lamp (FWHM<10 meV) and measured using a back-thinned CCD spectrometer PMA-11 (Hamamatsu) at room temperature. Fluorescence transients were measured using a time-correlated single photon counting system PicoHarp 300 (PicoQuant) utilizing a semiconductor diode laser (repetition rate 1 MHz, pulse duration 70 ps, emission wavelength 375 nm) as an excitation source. Fluorescence quantum yields (Φ_F) of the solutions were estimated using the integrated sphere method.[31] An integrating sphere (Sphere Optics) coupled to the CCD spectrometer via optical fiber was also employed to measure Φ_F of the films. Fluorescence concentration quenching effects of the DPA derivatives were analyzed by dispersing molecules in an inert polymer (polystyrene, PS) matrix and estimating Φ_F dynamics *vs* molecule concentration in the range of 0.05 – 100 wt %. The DPA derivatives dispersed in polystyrene films were prepared by dissolving the DPA derivatives and PS at appropriate ratios in THF solutions and then wet-casted the solutions on quartz substrates. Cyclic voltammetry experiments were performed on the Edaq ER466 Integrated Potentiostat System. Platinum wire, glassy carbon disk [Ø 1.6 mm, Ø 3.0 mm], and Ag/AgCl were used as counter, working, and reference electrodes, respectively. In all cases, CV experiments were performed in DMF (N,N – dymethylformamide) with tetrabutylammonium perchlorate - as supporting electrolyte (0.1 M) under Ar flow; concentrations of compounds were 0.002 M. The scan rate was 50 mV s^{-1}. Carrier drift mobility of the wet-casted neat films was measured by xerographic time of flight (XTOF) method.[32–34] The samples for the charge carrier mobility measurements were prepared as described earlier.[35] The film thickness was in the range of 3−6 μm. The ionization potentials (I_p) of the compound films were measured by electron photoemission in air method as described elsewhere.[36]

Materials.

DPA derivatives **1**-**6** (see Figure 1) were prepared according the scheme, presented in Figure 2. A substituted benzene was acylated by phthalic anhydride, the resulting substituted benzoylbenzoic acid underwent an intramolecular cyclization upon an action of an inorganic acid, what led to a formation of 2-substituted anthraquinone. It reacted with arylmagnesium bromide, the resulting 9,10-diaryl-9,10-dihydroxydihydroanthracene was reduced, thus forming 2,9,10-trisubstituted anthracene.

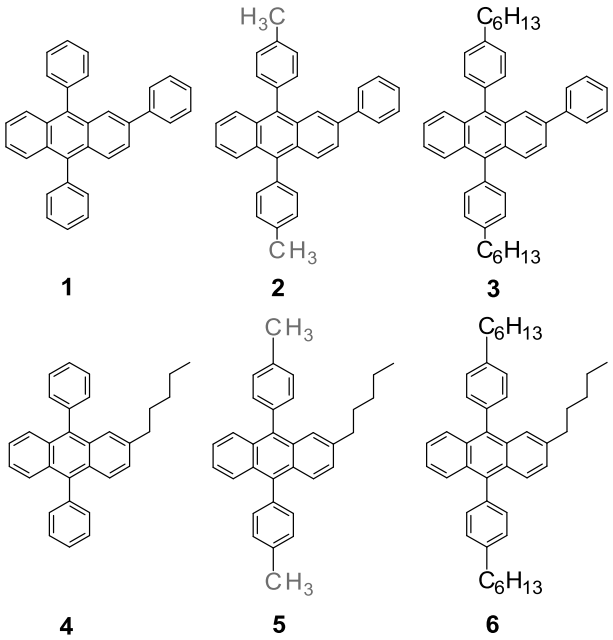

Figure 1. Chemical structures of the DPA derivatives studied in this work.

(4-Phenylbenzoyl)-2-benzenecarboxylic acid. 2 L glass bulb, equipped with mechanical stirrer, thermometer and reflux condenser, was placed in an ice bath and charged with 1.2 L dichlorethane, cooled down to 0 – 5^{0}C. On stirring 139 g (0.9 mol) biphenyl, 120 g (0.9 mol) aluminium trichloride and 133 g (0.9 mol) phthalic anhydride was added at such rate, that the temperature would maintain within 0 - +5^{0}C range. After all the reagents were introduced, the mixture was stirred still 0.5h, after this the ice bath was changed to a water bath and heated up to +40^{0}C. 120 g (0.9 mol) aluminium chloride was added portionwise, the temperature kept in 40-45^{0}C range. The released hydrogen chloride through reflux condenser was absorbed in sodium hydroxide solution. After all aluminium chloride was introduced, the reaction mixture was stirred at the same 40-45^{0}C for 2 h, then poured into an ice – 0.2L hydrochloric acid mixture. The solid product was filtered off, washed three times with water and dried at 100^{0}C. 253 g 2-(4-phenylbenzoyl)benzenecarboxylic acid was obtained, which was used in the next step without an additional purification.

2-Phenylanthraquinone. 2L glass bulb was charged with 800 g polyphosphoric acid and heated up to 160^{0}C, then in 20 min, 253 g (0.836 mol) 2-(4-phenylbenzoyl)benzenecarboxylic acid was added and stirred for 4.5 h at 160-166^{0}C. After this the mixture was cooled down to +140^{0}C and poured into 5 L hot water and left for a night to cool down. The mixture was filtered, the solid was placed into 10% aqueous potassium hydroxide solution, the mixture boiled for 0.5h, filtered, the solid washed by water, filtered again. The solid was extracted with 1.3 L toluene, concentrated, the remainder was distilled under vacuum, b.p. 220-275^{0}C/1 Torr. 126 g (0.443 mol) 2-phenylanthraquinone was obtained, yield 53%. M.p. 162-163^{0}C.

2-Pentylanthraquinone. 2-Pentylanthraquinone was prepared in a similar way, just the cyclization of 2-(4-pentylbenzoyl)benzenecarboxylic acid was carried out not in polyphosphoric acid, but in 5% oleum at 80^{0}C. M.p. 85^{0}C.

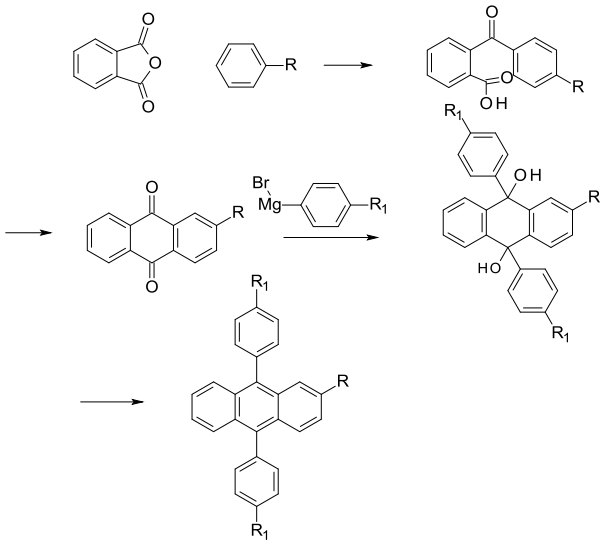

Figure 2. The synthesis scheme of the DPA derivatives **1-6**

2-Pentyl-9,10-bis(4-methylphenyl)anthracene. A round 250 ml glass bulb was charged with 3.19 g (0.131 mol) magnesium powder and 100 ml dry tetrahydrofuran. 21.4 g (0.125 mol) 4-bromotoluene was added dropwise at constant stirring, then refluxed for 3 h, till most of magnesium dissolved. A solution of 3.5 g (0.0125 mol) 2-pentylanthraquinone in 30 ml tetrahydrofuran was added to this mixture dropwise at room temperature, then the resulted mixture was refluxed for 4h. The mixture was cooled down to room temperature and poured into a saturated aqueous solution of ammonium chloride. The mixture was extrated by dichloromethane, an organic layer separated and evaporated.
To the residue 17 g (0.102 mol) potassium iodide, 14.7 g (0.167 mol) sodium dihydrophosphite and 50 ml anhydrous acetic acid was added and the whole mixture was heated at reflux for 3 h. The mixture was poured into water, extracted by dichloromethane and purified by column chromatography on silicagel, eluent toluene. The collected product was crystallized from acetone. 0.7 g (1.6 mmol) light yellow powder, m.p. 78-80^{0}C, was obtained, yield 13% from 2-pentylanthraquinone. GC-MS: M/z 428.3. $C_{33}H_{32}$, calculated: FW 428.61. ^{1}H-NMR (400 MHz, $CDCl_3$): δ 7.744-7.675 (m, 3H), 7.493-7.383 (m, 9H), 7.329-7.285 (m, 2H), 7.234-7.208 (dd, J_1=8.8 Hz, J_2=1.6 Hz, 1H), 2.658 (t, J=8 Hz, 2H), 2.575 (m, 6H), 1.607 (m, 3H), 1.318 (m, 3H), 0.890 (t, 3H). ^{13}C-NMR (400 MHz, $CDCl_3$): δ 139.36, 136.95, 136.86, 136.82, 136.20(2), 131.27, 131.22, 130.20, 129.57, 129.10, 129.07, 128.89, 127.02, 126.98, 126.93(2), 124.72, 124.69, 124.43, 36.27, 31.53, 30.81, 22.53, 21.45, 21.42, 14.04.
According to the same procedure the rest of 2,9,10-trisubstituted anthracenes were obtained.
2,9,10-Triphenylanthracene. Light yellow powder, crystallized twice from acetic acid and once from hexane. Yield 35%. M.p. 175-177^{0}C. GC-MS: M/z 406.3. $C_{32}H_{22}$, calculated: FW 406.52. ^{1}H-NMR (300 MHz, $CDCl_3$): δ 7.37-7.46 m, 5H), 7.57-7.88 (m, 16H), 7.98 (s, 1H). ^{13}C-NMR (300 MHz, $CDCl_3$): δ 124.8, 125.3, 125.4, 127.2, 127.3, 127.5, 127.6, 127.8(2), 127.9, 128.7, 129.1, 129.3, 130.3, 130.4, 130.6, 131.6, 131.7, 137.3, 137.6, 137.7, 139.2, 139.3, 141.4.
2-Phenyl-9,10-bis(4-methylphenyl)anthracene. Light yellow powder, crystallized from acetic acid and three times from hexane. Yield 22%. M.p. 209-211^{0}C.GC-MS: M/z 434.3. $C_{34}H_{26}$, calculated: FW 434.57. ^{1}H-NMR (300 MHz, $CDCl_3$): δ 7.98 (s, 1H), 7.87-7.29 (m, 19H), 2.58-2.59 (s, 6H). ^{13}C-NMR (300 MHz, $CDCl_3$): δ 141.5, 137.7, 137.5, 137.4, 137.3, 139.3, 136.2,

136.1, 131.4, 130.4, 129.4(2), 129.0, 127.9, 127.6, 127.4, 127.3, 125.2, 125.1, 124.9, 21.6.
2-Phenyl-9,10-bis(4-n-hexylphenyl)anthracene. Light yellow powder, crystallized from acetic acid and twice from hexane. Yield 26%. M.p. 105-107^{0}C.
GC-MS: M/z 574.5. $C_{44}H_{46}$, calculated: FW 574.84. ^{1}H-NMR (300 MHz, $CDCl_3$): δ 7.98 (s, 1H), 7.85-7.60 (m, 6H), 7.46-7.29 (m, 13H), 2.87-2.81 (t, J=1.2 Hz), 4H), 1.83 (m, 4H), 1.53-1.43 (m, 12H), 1.00 (t, J=2.4 Hz, 6H). ^{13}C-NMR (300 MHz, $CDCl_3$): δ 142.4, 142.3, 141.5, 137.8, 137.3, 137.2, 136.3, 136.2, 131.4, 130.7, 130.4, 129.4, 129.0, 128.7(2), 128.0, 127.6, 127.4, 127.3, 125.2, 125.1, 124.9, 36.2(2). 32.1, 31.8, 31.6, 29.4(2), 22.9, 14.4.
2-Pentyl-9,10-diphenylanthracene. Light yellow powder, crystallized from acetone, yield 28%. M.p. 87-89^{0}C. GC-MS: M/z 400.3. $C_{31}H_{28}$, calculated: FW 400.55. ^{1}H-NMR (400 MHz, $CDCl_3$): δ 7.725-7.572 (m, 9H), 7.522-7.518 (d, J=1.6 Hz, 4H), 7.501 (s, 1H), 7.450-7.215 (m, 3H), 1.612-1.580 (m, 4H), 1.326-1.289 (m, 4H), 0.881 (t, 3H). ^{13}C-NMR (400 MHz, $CDCl_3$): δ 139.50, 139.30, 139.26, 136.88, 136.23, 131.39, 131.33, 130.06, 130.04, 129.42, 128.75, 128.39, 128.36, 127.39, 127.34, 127.07, 126.94, 126.89, 126.84, 124.85, 124.59, 124.57, 36.24, 31.48, 30.71, 22.50, 14.02.
2-Pentyl-9,10-bis(4-n-hexylphenyl)anthracene. Light yellow powder, crystallized twice from acetone. Yield 23%. M.p. 64-65^{0}C. GC-MS: M/z 568.5. $C_{43}H_{52}$, calculated: FW 568.87. ^{1}H-NMR (400 MHz, $CDCl_3$): δ 7.744- 7.675 (m, 3H), 7.482-7.394 (m, 9H), 7.330-7.286 (m, 2H), 7.234-7.208 (m, 1H), 2.852-2.797 (q, J= 8 Hz, 4H), 2.687-2.649 (t, J=7.2 Hz, 2H), 1.851-1.795 (m, 4H), 1.639-1.575 (m, 2H), 1.511-1.298 (m, 17H), 0.995-0.906 (2t, 9 H). ^{13}C-NMR (400 MHz, $CDCl_3$): δ 142.02, 141.91, 139.26, 136.89, 136.38, 136.36, 136.25, 131.22, 131.18, 130.20(2), 129.58, 128.91, 128.36,128.34, 127.06, 127.00, 126.96, 126.91, 124.69, 124.41, 36.21, 35.95, 31.83, 31.54, 31.48, 30.66, 29.21, 29.19, 22.69, 22.53, 14.15, 14.04.

Computational methods

Quantum chemical calculations of the DPA derivatives were performed using density functional theory B3LYP method implemented in the Gaussian09 software package.[37] Ground-state geometries of molecular structures were optimized in a 6/31G basis set. Electronic excitation energies, oscillator strengths of the singlet and triplet transitions and spatial distributions of electron density for HOMO and LUMO for „freezed“ structures were calculated using semiempirical ZINDO procedure (for singlets only and for triplets only, respectively).

Results and discussion

Theoretical calculations.

Figure 3 demonstrates spatial electron density distribution in the HOMO and LUMO of the DPA derivatives **1-6** with optimized geometry. Phenyl groups at the 9th and 10th positions in the unsubstituted DPA are known to form right angle with the anthracene core, whereas in the studied nonsymmetrically substituted DPA compounds **1-6** this angle in some cases reduces to about 80°. 2-phenyl group in the compounds **1-3** is twisted in respect to the core by about 55°. Generally, the spatial distribution of electron density in the ground and excited states resemble that of the unsubstituted anthracene.[38] Only a small fraction of molecular orbitals extends

towards the substituents. This extension towards 2-phenyl group is somewhat more noticeable than towards the 9,10-phenyls.

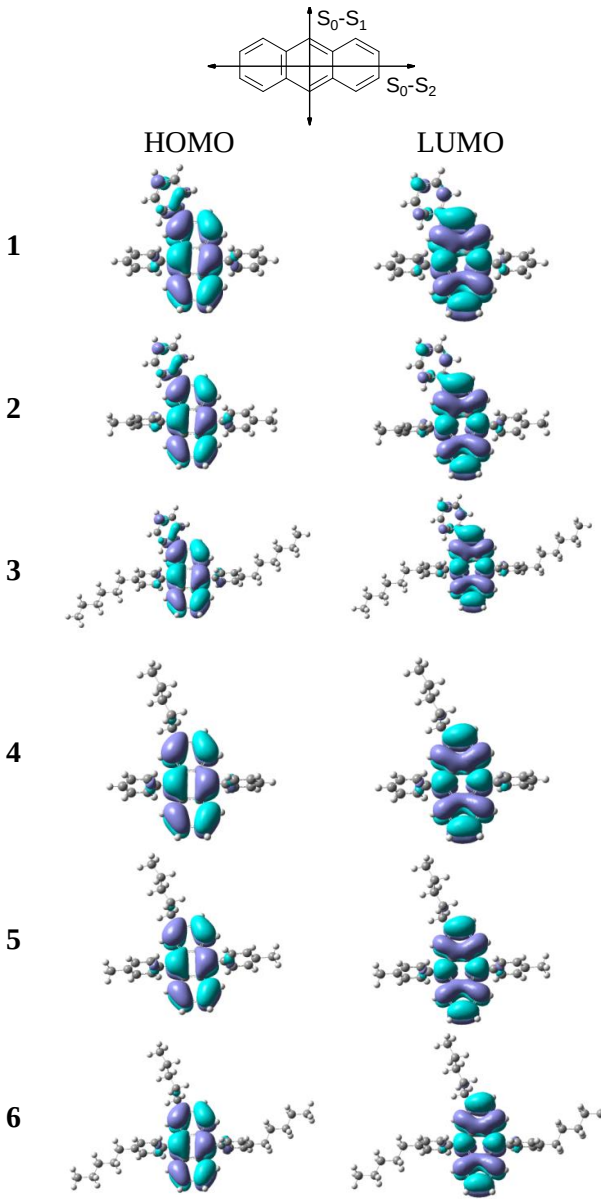

Figure 3. HOMO and LUMO of the DPA compounds **1**-**6** calculated using the B3LYP/6-31G basis set. The position of the short (denoted as S_0-S_1) and long (denoted as S_0-S_2) molecular axis of anthracene molecule is denoted in the top picture.

The $S_0 \rightarrow S_1$ optical transition dipole moment of the anthracene lies along the short axis of the molecule, while the transition dipole moment of $S_0 \rightarrow S_2$ lies along the long axis. Therefore, introduction of various substituents at the 9^{th} and 10^{th} positions increases oscillator strength of the $S_0 \rightarrow S_1$ optical transitions, whereas the modifications at 2, 3, 6 and 7 positions mainly affect the $S_0 \rightarrow S_2$ transition. Table 1 displays calculated oscillator strengths and energies of the lowest singlet and triplet transitions of the DPA derivatives **1**-**6** and of the unsubstituted DPA. The $S_0 \rightarrow S_1$ transition energy of the DPA is estimated to be 3.14 eV. The energy reduces down to

3.115-3.124 eV with the introduction of 2-pentyl substituent (compounds **4**-**6**) and slightly more down to 3.069-3.091 eV with the introduction of more conjugated 2-phenyl substituent (compounds **1**-**3**). Calculated energies of the two lowest triplet states T_1 and T_2 of the DPA derivatives correlated well with the first singlet transition energies and were found to depend on the substitution at the 2nd position. For the compounds **4**-**6** possessing 2-pentyl substituent the triplet energies were rather similar to those of the unsubstituted DPA (0.995/2.05 eV for T_1/T_2), whereas for the compounds **1**-**3** the T_1/T_2 energies were somewhat lower (0.98/1.9605 eV for T_1/T_2) due to the more conjugated 2-phenyl group. Although the differences in singlet and triplet energies of the compounds **1**-**3** and **4**-**6** are not significant, they can notably affect the rate of intersystem crossing thereby severely impacting photophysical and photoelectrical properties of the compounds. The oscillator strength of the dominating singlet transitions $S_0 \rightarrow S_1$ was found to be at least 4 times as large as that of the nearest $S_0 \rightarrow S_2$ transitions. The oscillator strength of $S_0 \rightarrow S_1$ transition of the DPA derivatives **1**-**6** showed variations depending on the nature of substituents. The highest oscillator strength was obtained for the unsubstituted DPA (0.376) and for 2-pentyl-substituted compounds (0.361-0.388), meanwhile 2-phenyl-substituted DPA derivatives exhibited slightly lower oscillator strength (0.326-0.361). The oscillator strength was slightly larger for the DPA compounds with longer alkyl groups attached at the *para* position of 9,10-phenyls due to the increased dipole moment of the $S_0 \rightarrow S_1$ transition. In contrast, the largest oscillator strength of the $S_0 \rightarrow S_2$ transition (having the dipole moment oriented along the longer molecular axis) was found for the 2-phenyl-substituted derivatives as compared to 2-pentyl-substituted analogues.

Table 1. Calculated transition energies for $S_0 \rightarrow S_1$ and $S_0 \rightarrow T_1$ /T_2, and oscillator strengths for $S_0 \rightarrow S_1$ and $S_0 \rightarrow S_2$.

	Compd.	Transition energy of $S_0 \rightarrow S_1$ (eV)	Transition energy of $S_0 \rightarrow T_1$ /T_2 (eV)	Oscillator strength of $S_0 \rightarrow S_1$	Oscillator strength of $S_0 \rightarrow S_2$
2-phenyl	**1**	3.091	0.981/1.956	0.326	0.09
	2	3.069	0.98/1.96	0.356	0.093
	3	3.076	0.98/1.959	0.361	0.093
2-pentyl	**4**	3.124	0.994/2.037	0.361	0.067
	5	3.115	0.996/2.032	0.385	0.067
	6	3.12	0.995/2.027	0.388	0.068
	DPA	3.14	0.995/2.053	0.376	0.072

Figure 4 illustrates the optimized geometry as well as total energy and oscillator strength of the compounds **3** and **6**. The total energy and oscillator strength as a function of dihedral angle β (between the anthracene core and the phenyl substituents at 9th and 10th positions) is shown in Figure 4 (b). Since the twist angle of the labile phenyl group at the 2nd position of anthracene was previously shown to have a small effect on the transition energies and oscillator strengths,[39] the angle β served as the main reaction coordinate in the geometry optimization of the DPA compounds. The optimization of the total energies indicated flat energy minima of S_0 state in respect to the angle β persisting from about 70° to 110°, whereas S_1 state exhibited two slightly

nonsymmetrical energy minima at the angles β of 70° and 110°. The barrier height between the minima was about 40 meV, which is close to the thermal energy (25 meV) at room temperature. The asymmetry in energy minima are obviously caused by the nonsymmetrical substitution of the DPA compounds. The oscillator strengths had minima at the right angles β, though a rapid increase of the strengths was clearly observed with a larger deviation from this angle.
Thus theoretical calculations show that substitution at the 2nd position of DPA by phenyl or pentyl moieties weakly perturbs electronic transitions, while 2,9,10-substitution ensures complex geometry of the molecules, which can significantly influence film-forming and thereby charge transport properties.

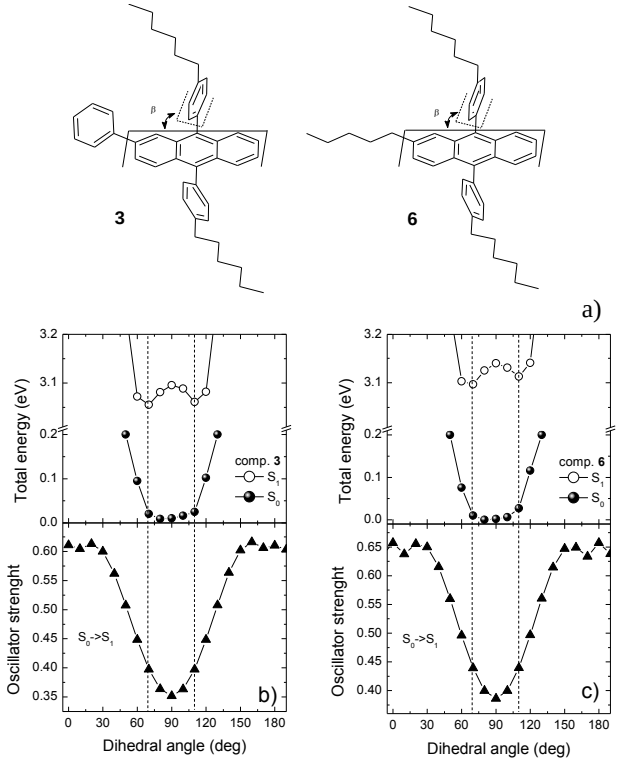

Figure. 4 (a) Molecular structures of the compounds **3** and **6**. β, dihedral angle between the planes of anthracene and 4-hexylphenyl substituents. Bottom graphs: calculated total energy of the ground state S_0 and the first excited state S_1 (upper picture) and oscillator strength of the $S_0 \rightarrow S_1$ transition (lower picture) as a function of dihedral angle β for the compound **3** (b) and compound **6** (c). Vertical dashed lines marks energy minima of S_1 state.

Thermal properties.

Thermal properties of the nonsymmetric DPA derivatives were assessed by utilizing DSC. Melting (T_m) and glass transition (T_g) temperatures of the derivatives are summarized in Table 2. The typical DSC curves for the compounds **2** and **5** are presented in Figure 5 and the rest of the thermograms are presented in Figure S1 in the Supporting Information.

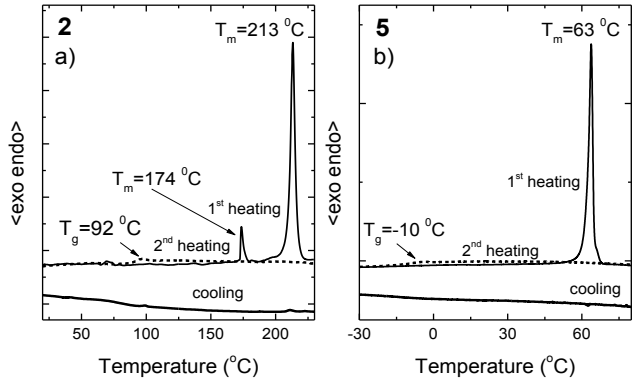

Figure. 5 DSC curves of the DPA compounds **2** (a) and **5** (b).

Melting (T_m) and glass transition (T_g) temperatures of the derivatives are summarized in Table 2. The typical DSC curves for the compounds **2** and **5** are presented in Figure 5.
All the DPA compounds **1**-**6** exhibited similar DSC thermograms by demonstrating melting signal only in the first heating scan with peaks centered at 101-209 ℃ and 60-86 ℃ for compounds **1**-**3** and **4**-**6**, respectively. The additional low intensity melting signals at 174 ℃ and 106 ℃ were observed for compounds **2** and **3**, respectively, which are possibly due to the presence of different crystalline phase. An absence of crystallization peaks during the cooling indicated that the compounds were transformed into an amorphous phase. The second heating scan revealed glass transition temperatures of 7-92 ℃ for compounds **1**-**3** and -24-(-1) ℃ for compounds **4**-**6.** The introduction of 2-pentyl substituent remarkably lowered the T_m and T_g. The continuous decrease of T_m and T_g was also observed with the increasing length of the alkyl groups attached at 9,10-phenyls. It should be noted, that fluorescence measurements above the T_g temperature for samples **3**-**6** had just minor impact on its properties (see Figure S2 in the Supporting Information)

Table 2. Thermal properties of DPA derivatives **1**-**6**.

Comp.	T_m (℃) [a]	T_g (℃) [b]
1	209	71
2	213	92
3	101	7
4	86	-1
5	63	-10
6	60	-24

[a] Melting temperature.
[b] Glass transition temperature

Absorption and fluorescence spectra.

Absorption and emission spectra of the dilute solutions and neat films of the DPA derivatives **1**-**6** are displayed in Figure 6. The detailed optical properties of all the derivatives and also of the unsubstituted DPA, which served as the reference compound, are summarized in Table 3. Note that for the compounds **3**-**6** optical measurements were performed at temperature exceeding their glass transition temperature. Absorption spectra of the DPA compounds **1**-**6** contain clearly

resolved vibronic structure with the dominant 1st vibronic replica similarly to that observed in the spectra of unsubstituted DPA (see Figure S3 in the Supporting Information) or other various DPA derivatives due to the presence of rigid anthracene core.[40–42] Nonsymmetric substitution at the 2nd position obviously increases lability of the anthracene structure thus making vibronic replica less pronounced.[40] The lowest energy vibronic bands in the absorption spectrum of the 2-phenyl substituted DPA compounds **1**-**3** peaks at 405 nm, whereas the bands of the 2-pentyl substituted counterparts **4**-**6** are shifted more in the UV (at about 391 nm) due to the worse π-conjugation of the substitutent. The molar extinction coefficient of the derivatives does not exceed that of the unsubstituted DPA (ε = 13400 L·mol^{-1}·cm^{-1}) and varies between 10000 and 13000 L·mol^{-1}·cm^{-1}.

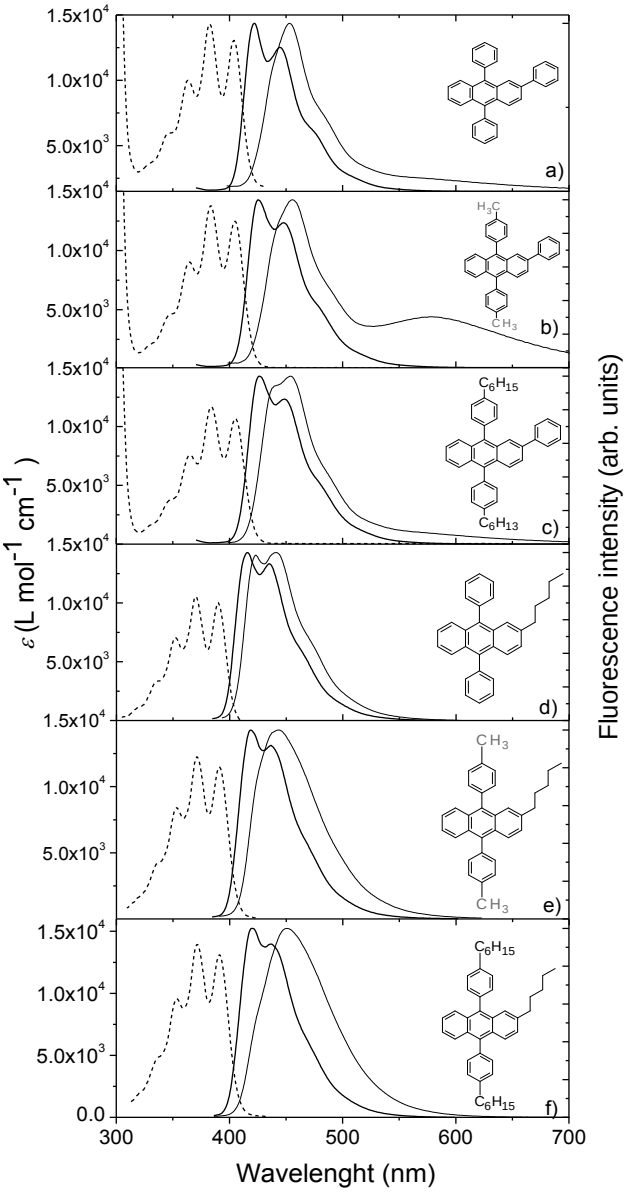

Figure. 6 Absorption (dashed line) and fluorescence (solid line) spectra of the DPA derivatives **1** (a), **2** (b), **3** (c), **4** (d), **5** (e) and **6** (f) in dilute 10^{-6} M THF solutions and neat films (thin solid lines).

Emission spectra of the DPA compounds **1**-**6** in the dilute solution also express vibronic bands, however a lack of the mirror images between absorption and emission implies flexibility of the molecules and geometrical transformations occurring in the excited state in agreement with DFT calculation results. In accordance with the absorption spectra, fluorescence bands of more conjugated 2-phenyl-substituted DPA derivatives **1**-**3** are located at 422-426 nm, and thus are slightly redshifted as compared to those of the less conjugated 2-pentyl-substituted DPA counterparts **4**-**6** peaking at 416-421 nm. To compare, 0^{th} vibronic replica of the unsubstituted DPA in a solution was observed at 409 nm.

Table 3. Absorption and fluorescence data of the DPA derivatives **1**-**6** and unsubstituted DPA in dilute (~10^{-6} M) THF solutions and neat films

	Dilute solution			Neat film
Compd.	λ_{abs}^{max} (nm) [a]	ε (l mol^{-1}cm^{-1}) [b]	λ_{FL}^{max} (nm) [c]	λ_{FL}^{max} (nm) [d]
1	363, 383, 404	13000	422	453
2	365, 384, 405	12500	425	456
3	365, 384, 405	10700	426	454
4	352, 370, 390	10050	416	441
5	353, 371, 391	11500	419	444
6	353, 372, 391	13100	421	450
DPA	355, 374, 394	13430	410	441

[a] Absorption band maximum.
[b] Molar absorption coefficient of the 0^{th} vibronic transition maximum.
[c] Fluorescence band maximum of dilute THF solution.
[d] Fluorescence band maximum of neat film.

Fluorescence spectra of the neat films of the DPA derivatives **1**-**6** are slightly redshifted as compared to the spectra of their dilute solutions, which is due to the enhanced intermolecular interactions in the solid state. The films of the compounds **1**-**3** and **4**-**6** emit in the deep blue with maxima positioned at 453-456 nm and 441-450 nm, respectively. CIE color coordinates of the emitters are displayed in Figure S4 in the *Supporting Information*. Noticeable vibronic structure in the fluorescence bandshapes of the DPA derivatives **1**-**4** points out dense molecular packing in the films, whereas nearly structureless shapes observed for the compounds **5**-**6** implies more random molecular arrangement, which is typical for amorphous films. Weak long-wavelength tail observed in the fluorescence spectra of compounds **1**-**3**, which is especially well pronounced in the compound **2** showing a small shoulder at 580 nm, is likely caused by excimer states formed as a result of denser molecule packing of the 2-phenyl-substituted DPA. Excimer bands typically lower fluorescence quantum yield (Φ_F), which is exactly the case of compounds **1**-**3**, yielding 5 to 10 times lower Φ_F as compared to that of **4**-**6** compounds bearing 2-pentyl substituents (see Table 4). This also adversely affects color purity of the films by shifting color coordinates closer to the white point of the chromaticity diagram.

Thus, in spite of enhanced electron-vibronic interaction, introduction of poorly-conjugated substituents at the 2nd position weakly affects electronic transition energies ensuring deep-blue emission both in noninteracting molecules and aggregate state. The small differences in transition energies, however might result in dramatic changes of excited state relaxation pathways.

Excited state relaxation.

Estimated fluorescence quantum yields (Φ_F) of the DPA derivatives in dilute solutions were found to range from 0.45-0.49 for compounds **1**-**3** to 0.68-0.71 for compounds **4**-**6** (see Table 3). As compared to Φ_F of the unsubstituted DPA, which is close to 1.0, significantly lower quantum yields of the DPA derivatives indicate moderately high rate of the nonradiative recombination processes. It is known that in planar and rigid molecules like anthracene, the nonradiative decay is caused entirely by the intersystem crossing to triplet states.[43,21] Efficient intersystem crossing results from the proximity of higher-lying triplet states (T_2 or higher) and singlet state S_1. For example, in the case of crystalline anthracene, the S_1 is located below the T_1 level, and thus Φ_F is increased to almost 1.0. Simple alteration of the anthracene core, like introduction of phenyl groups at 9th and 10th positions, as in 9,10-diphenylanthracene, can easily realign singlet and triplet energies resulting in close to unity quantum yields.[30] However, conversion of the symmetric DPA structure to nonsymmetric, for instance, by additional substitution at the 2nd position with phenyl group (compounds **1**-**3**) might not only affect energy alignment, but also enhance electron-vibronic coupling, which can efficiently deactivate excited state via nonradiative intramolecular torsions.[44,45] Indeed, 2-phenyl-substituted DPA compounds **1**-**3**, exhibit somewhat lower fluorescence efficiencies as compared to those of 2-pentyl-substituted analogues suggesting the presence of the torsional motions. To discriminate between the two effects additional experiments, where one of the effects is fully eliminated, are needed. The results of these experiments will be discussed below.

Φ_F of the neat films of the DPA derivatives were found to be considerably lower as those of their dilute solutions. Φ_F values of only 0.03-0.06 were obtained in 2-phenyl-substituted DPA compounds **1**-**3**, whereas 0.27-0.42 values were estimated for the **4**-**6** compounds with 2-pentyl groups. Intermolecular interactions in the films, which are known to promote exciton migration, and thus enhance the possibility for the excitons to be captured by the quenching sites (lattice distortions, impurity traps or other defects) are responsible for this Φ_F lowering and depend on intermolecular separation. Obviously, only 2-fold drop in Φ_F observed for the neat films of compounds **4**-**6** as compared to their solution in contrast to roughly 10-fold drop observed for the compound **1**-**3** neat films indicates that the 2-pentyl moieties more effectively suppress aggregate formation as the 2-phenyl groups. This result is well supported by the long-wavelength tails observed in the fluorescence spectra of the neat films of compounds **1**-**3** being attributed to the excimer emission (see Figure 6) and signifying reduced average intermolecular distance.

Excited state relaxations dynamics of the DPA derivatives was assessed by measuring fluorescence decay transients. The transients of the compound dilute solutions and neat films are shown in Figure 7, whereas extracted fluorescence lifetimes (τ_F) are listed in Table 4. Fluorescence transients of the DPA derivatives **1**-**6** in dilute solutions follow single-exponential decay profile with τ_F of 5.0-6.2 ns similar to that of the unsubstituted DPA (τ_F=6.0 ns). In contrast, fluorescence transients of the neat DPA films exhibit highly non-exponential decay profiles. The non-exponential temporal profile accompanied by the redshifted fluorescence bands

of the solid films is a clear signature of energy transfer occurring via exciton hopping through the localized states in disordered or partly disordered media.[46,47] The fluorescence decay profiles were fitted by using three-component exponential decay model to reveal the major component (see Table 4). The fractional intensity of each component, which signifies the actual contribution of the component to overall excited-state decay, is indicated in the brackets next to the τ_F value. Considerably faster excited state decay of the compound neat films as compared to that of solutions indicated enhanced excitation migration and migration-assisted nonradiative relaxation at the quenching sites.

To evaluate the contribution of radiative and nonradiative relaxation rates and to reveal the dominant mechanisms determining differences in the optical properties of the compounds **1**-**3** and **4**-**6**, radiative (τ_r) and nonradiative (τ_{nr}) decay time constants were calculated (see Table 3). The time constants were calculated using the following relations:

$$\tau_r = \tau_F / \Phi_F, \quad \tau_{nr} = \tau_F / (1 - \Phi_F), \qquad (1)$$

where the term τ_{nr} takes into account all the possible nonradiative decay pathways including intersystem crossing to triplet states, which is considered to be very important in the anthracene-based compounds.[1,48]

Alteration of intersystem crossing rate.

Despite the similar fluorescence lifetimes of the two series of DPA derivatives **1**-**3** and **4**-**6** in solution, the series show different behavior of the radiative and nonradiative relaxation processes. Radiative decay time of the compounds is rather similar, i.e. average τ_r is 10.8 ns and 8.5 ns for the compound series **1**-**3** and **4**-**6**, respectively, whereas nonradiative time constant of these series differ by a factor of 2. τ_{nr} is found to be significantly shorter, and so the nonradiative relaxation rates faster, for the 2-phenyl-substituted DPA compounds **1**-**3** ($\tau_{nr} \approx 9.7$ ns) as compared to those bearing 2-pentyl moiety, compounds **4**-**6** ($\tau_{nr} \approx 18.9$ ns). The 2-fold enhancement of nonradiative decay rates in the compounds **1**-**3** can be associated with the intensified intramolecular torsions induced by the twisted phenyl group attached at the 2nd position of the DPA core, although τ_{nr} enhancement may also be promoted by the enhanced intersystem crossing rate due to the 2-phenyl substituent, which can invoke better triplet and singlet energy alignment. To differentiate between the two possible mechanisms, the DPA compounds were dispersed in a rigid polystyrene (PS) matrix at low mass percentage (0.1 wt %). Such low molecular concentration in the matrix prevented the DPA molecules from interacting while simultaneously inhibited their intramolecular motions. Estimated fluorescence lifetimes, quantum yields, radiative and nonradiative decay time constants for the DPA derivatives **1**-**6** as well as for the unsubstituted DPA in PS matrices are summarized in Table 3 for comparison. Fluorescence decay transients of the DPA derivatives **1**-**6** dispersed in polystyrene (PS) matrix are provided in Figure S5 in the Supporting Information.

It is worth noting that the fluorescence quantum yield of the unsubstituted DPA in solution and rigid PS matrix is nearly the same and approaches 100%. This unambiguously indicates that phenyl moieties at the 9,10- positions of the DPA core are not involved in torsional motions, and thus, do not contribute to the nonradiative deactivation of the excited state. This is explained by perpendicular orientation of the 9,10-phenyls in respect to the core, which ensures their stiffness and resistance to twisting. Consequently, only the phenyl group linked to the DPA core at the 2nd position could invoke nonradiative deactivation *via* the intramolecular torsions. A comparison of

the Φ_F of the compounds **1**-**3** with the 2-phenyl moieties in dilute solution and PS matrix shows slight increase of the Φ_F in the rigid matrix (from ~0.47 in solution to ~0.60 in PS matrix) mainly due to the decreased nonradiative decay time. However a similar increase of Φ_F is also observed for **4**-**6** derivatives without these moieties (from ~0.69 in solution to ~0.84 in PS matrix), where torsional motions are absent. This result clearly rules out the intramolecular torsions as the key-mechanism responsible for enhanced nonradiative relaxation of the compounds **1**-**3** and suggests enhanced intersystem crossing to triplet states to play the decisive role. As in the case of solutions, τ_r of the DPA derivatives **1**-**3** and **4**-**6** in PS matrix are estimated to be rather similar, 12 ns and 10.7 ns, respectively, whereas τ_{nr} of the compounds **1**-**3** are found to be up to 4 times shorter as those of the compounds **4**-**6**. Similarly to the compound solutions, enhanced nonradiative relaxation in PS matrices for compounds **1**-**3** can be attributed to the 2-phenyl moieties induced enhanced intersystem crossing to triplet states. In the case of 2-pentyl groups, most likely the misalignment of the first singlet and higher-lying triplet states is larger making the intersystem crossing rate not so efficient. This results in longer τ_{nr} and thus higher Φ_F.

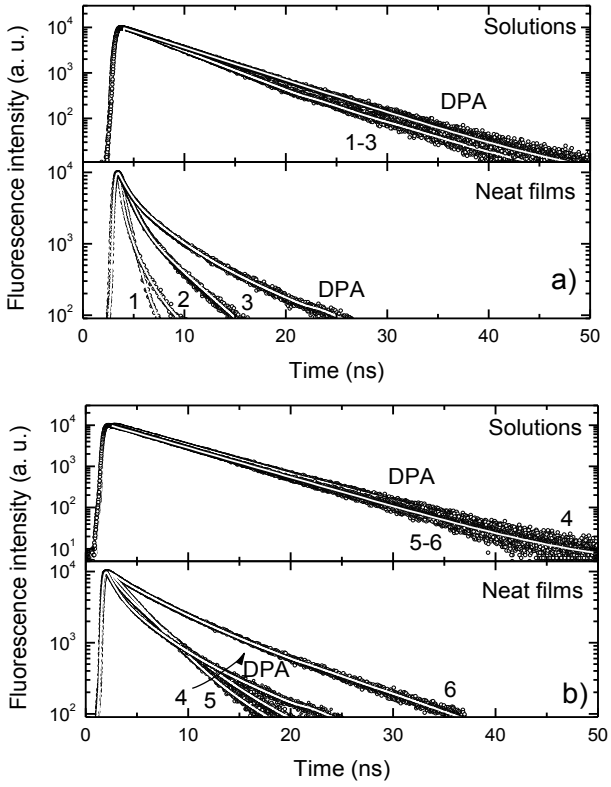

Figure 7. Fluorescence transients of DPA derivatives in THF solutions and neat films. Lines indicate single or double exponential fits to the experimental data. a) Compounds **1**-**3**. b) Compounds **4**-**6**. Excitation wavelength is 375 nm (repetition rate 1 MHz, pulse duration 70 ps).

The importance of the nonsymmetric substitution at the 2nd position of the DPA derivatives to the optical properties can be confirmed by comparing their radiative and nonradiative decay rates (or time constants) with those of the reference compound, unsubstituted DPA. The radiative decay time of the solutions of DPA derivatives bearing either 2-phenyl or 2-pentyl moieties differs by less than twice as compared to that of the reference DPA. Meanwhile the difference in

nonradiative decay time of all the derivatives in respect to the reference is dramatic, i.e. τ_{nr} is one order of magnitude shorter for the compounds with 2-phenyl moieties (**1**-**3**) and 5 times shorter for those with 2-pentyl moieties (**4**-**6**). An analogous behavior of τ_r and τ_{nr} in respect to those of the reference DPA is also observed for the DPA derivatives in PS matrix. This result again verifies the importance of the type of substituent linked to the 2nd position of the DPA in governing the nonradiative relaxation processes via the intersystem crossing to triplet states. The influence of the alkyl group length attached at the *para* position of 9,10-phenyls on the optical properties of the DPA derivatives in dilute solution or polymer matrix is insignificant. The alkyl groups become by far important in the film formation, fluorescence concentration quenching and carrier transport properties as it will be discussed below.

Table 4. Fluorescence decay time constants, quantum yields, radiative and nonradiative decay time constants of the DPA derivatives **1-6** in 10^{-6} M THF solutions, neat films and 0.1 wt % in PS films.

	Compd.	Dilute solution				Neat film		PS matrix (0.1 wt% in PS)			
		τ_F (ns) [a]	τ_r (ns) [b]	τ_{nr} (ns) [c]	Φ_F [d]	τ_F (ns) [e]	Φ_F [d]	τ_F (ns) [a]	τ_r (ns) [b]	τ_{nr} (ns) [c]	Φ_F [d]
2-phenyl	**1**	5.2	11.6	9.5	0.45	0.45 [70%] 0.95 [26%] 4.09 [4%]	0.06	8	14.5	17.8	0.55
2-phenyl	**2**	5.1	10.6	9.7	0.48	0.24 [57%] 1.07 [30%] 3.48 [14%]	0.03	6.45	10.9	15.3	0.59
2-phenyl	**3**	5	10.2	9.8	0.49	0.83 [55%] 3.41 [45%]	0.06	6.96	10.7	19.9	0.65
2-pentyl	**4**	6.2	9.1	19.4	0.68	1.03 [13%] 2.98 [82%] 12.48 [6%]	0.27	9.69	11	80.8	0.88
2-pentyl	**5**	5.8	8.5	18	0.68	0.66 [9%] 3.05 [76%] 8.55 [15%]	0.3	8.75	11.1	41.7	0.79
2-pentyl	**6**	5.6	7.9	19.3	0.71	1.15 [7%] 5.86 [76%] 16.56 [18%]	0.43	8.36	10	51.3	0.84
	DPA	6	6.4	100	0.94	0.64 [17%] 2.66 [44%] 7.62 [39%]	0.26	8.1	8.3	405	0.98

[a] Fluorescence decay time.
[b] Radiative decay time.
[c] Non-radiative decay time.
[d] Fluorescence quantum yield.
[e] Fluorescence decay time of neat films.

Fluorescence concentration quenching.

Fluorescence concentration quenching is a key factor, which determines the applicability of a compound for OLED application.[49,50] Utilization of an emissive material at high concentrations (typically of more than a few percent) in a host material is limited by the enhanced molecule interaction, and in severe cases, physical molecule agglomeration activating exciton migration and migration-induced exciton quenching, and therefore is detrimental to the device performance.[51,52] Concentration quenching in the DPA derivatives was evaluated by dispersing DPA molecules in a rigid and transparent polystyrene (PS) host while measuring fluorescence quantum yield changes *vs* concentration in the broad range of concentrations 0.1-100 wt % (see Figure 8). All the DPA derivatives **1**-**6** demonstrated negligible fluorescence concentration quenching up to 8 wt % in PS. The rate of concentration quenching for the compounds **1**-**3** featuring 2-phenyl substituent is very similar (Figure 8a). Φ_F quenches just lightly faster as compared to that of the unsubstituted DPA. Conversely, concentration quenching of the compounds **4**-**6** possessing 2-pentyl substituent is found to be dependent on the alkyl group length (Figure 8b). The shorter alkyl groups attached at the 9,10-phenyls of the DPA results in more rapid quenching as compared to the longer groups. This is evidently caused by the reduced intermolecular separation, and thus enhanced intermolecular interaction, due to the smaller alkyl spacers. Importantly, the quenching with increasing the concentration of 2-pentyl-substituted DPA compounds **4**-**6** in PS matrix is slower as compared to that of the reference DPA, and moreover, slower than that of 2-phenyl substituted DPA **1**-**3**. The obtained results highlight a significance of the 2-pentyl moieties in more effective suppression of intermolecular interaction resulting from looser molecular packing as that caused by the 2-phenyl groups.

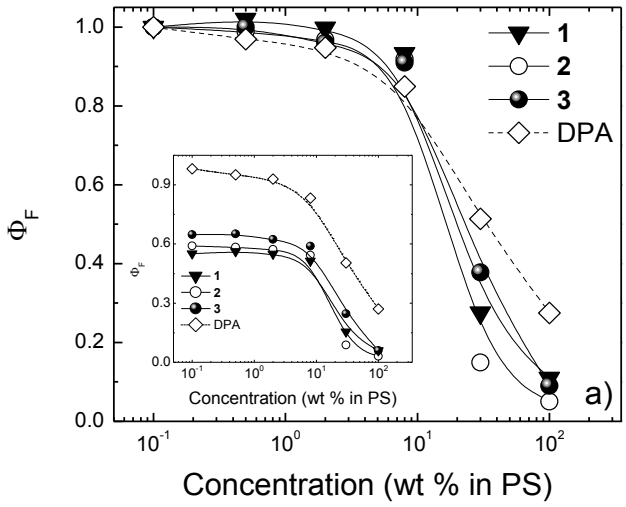

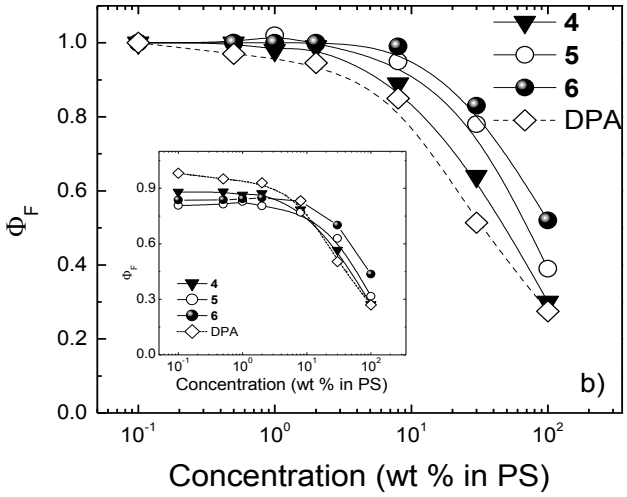

Figure 8. Normalized fluorescence quantum yield of the DPA compounds **1**-**3** (a) and **4**-**6** (b) as a function of their concentration in PS matrix. Lines are guides to the eye. Absolute values of fluorescence quantum yields are displayed in insets.

Electrochemical properties.

Cyclic voltammetry was employed to elucidate the energies of HOMO and LUMO of the DPA derivatives **1**-**6** (see Figure 9 and Table 5). All the compounds demonstrated non-reversible oxidation-reduction processes by applying low scan rate (50 mV/s) in the range of positive potentials. For the compounds **2** and **3**, a quasi-reversible oxidation-reduction potential was observed after the scan rate was increased to 200 mV/s, whereas in the range of negative potentials quasi-reversible oxidation-reduction potentials were observed for all the DPA compounds independently on the scan rate.

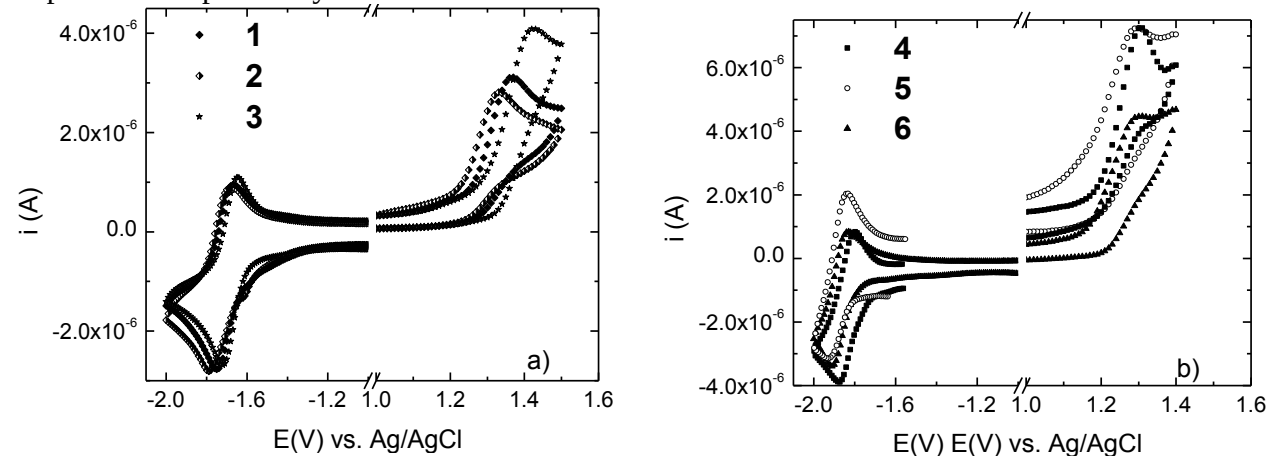

Figure 9. Cyclic voltammograms of the dilute solutions of compounds **1**-**3** (a) and **4**-**6** (b) in N,N – Dymethylformamide at 50 mV/s scan rate. Compound concentration was 0.002 M with tetrabutylammonium perchlorate (0.1 M) used as the electrolyte.

1-**3** and **4**-**6** series of the derivatives exhibited rather similar HOMO energies, ~5.28 eV and ~5.32 eV, respectively, whereas somewhat greater variation in LUMO energies between the series was obtained. The compounds **1**-**3** showed lower LUMO levels (~2.56 eV) as compared to

the levels (~2.42 eV) estimated for the compounds **4-6** (see Table 5). The decreased LUMO energy observed for the compounds bearing more conjugated 2-phenyl substituent is likely a cause of the lower Φ_F due to the enhanced intersystem crossing rate.

Table 5. Electrochemical properties (oxidation and reduction potentials, energies of HOMO and LUMO levels, electrochemical and optical bandgaps) of the DPA derivatives **1**-**6**.

Comp.	$E_{FC}^{1/2}$ (eV) [a]	E_{ox} onset (eV) [b]	E_{red} (eV) [c]	E_{HOMO} (eV) [d]	E_{LUMO} (eV) [e]	E_g^{el} (eV) [f]	$E_g^{opt.}$ (eV) [g]
1	0.52	1.03	-1.71	-5.31	-2.58	2.72	2.94
2		0.98	-1.73	-5.26	-2.55	2.74	2.94
3		0.99	-1.73	-5.27	-2.56	2.72	2.93
4		1.11	-1.84	-5.39	-2.45	2.94	3.07
5		1	-1.88	-5.28	-2.4	2.88	3.04
6		1.03	-1.88	-5.31	-2.41	2.91	3.04

[a] Half – wave potential vs. Ag/AgCl for reversible oxidation reduction of ferrocene.
[b] On-set of oxidation potential for HOMO level.
[c] Half – wave potential vs. Ag/AgCl for LUMO level.
[d],[e] HOMO and LUMO energy, $E_{HOMO}/E_{LUMO} = -(4{,}8 + E_{ox}^{\frac{1}{2}}/E_{red}^{\frac{1}{2}} - E_{FC}^{1/2})$.
[f] Electrochemical bandgap, $|Eg_{el}|=|E_{LUMO}|-|E_{HOMO}|$.
[g] Optical bandgap, estimated from the onset of the absorption band.

Charge transport properties and ionization potential.

Achieving high carrier mobility in the amorphous films requires a good balance of the film forming properties and charge carrier transfer rate. The impact of alkyl group length (C0, C1 and C6) on the charge transport properties of the two nonsymmetrically-substituted DPA compound series bearing 2-phenyl (compounds **1, 2, 3**) and 2-pentyl moieties (compounds **4, 5, 6**) was investigated. The wet-casted amorphous films of the DPA derivatives were investigated by using XTOF method. The reference DPA was found to form polycrystalline neat films with low photosensitivity, which made XTOF measurements practically impossible. Introduction of the additional phenyl or pentyl moieties at the 2nd position and the methyl groups at the *para* positions of 9,10-phenyls (compounds **1**, **2**, **4**, **5**) completely suppressed DPA crystallization and ensured formation of amorphous neat films. It is worth emphasizing that these modified nonsymmetric DPA derivatives expressed very high hole drift mobilities (μ_h) well exceeding 10^{-3} cm^2/Vs at 1 MV/cm electric field. The obtained drift mobility values varied from $4.6\cdot10^{-3}$ cm^2/Vs in the compound **1** up to almost $1\cdot10^{-2}$ cm^2/Vs in the compound **4** at an electric field of 1 MV/cm (see Figure 10 and Table 6). XTOF transients measured at different voltages are displayed in Figure S6 in the *Supporting Information*. Although alkyl groups at the *para* positions of 9,10-phenyls negligibly affected optical properties of the DPA compounds, their length severely altered molecular packing, and thus charge carrier transport properties. Introduction of methyl group (compound **2**) slightly enhanced hole drift mobility and increased glass transition temperature, whereas analogous substitution for the compounds possessing 2-pentyl moiety, worsened the drift mobility and glass transition temperature. This can be

attributed to the better steric hindrance effect of the twisted 2-phenyl substituent. Further extension of the alkyl group length up to C6 atoms (compounds **3** and **6**) strongly impaired film forming properties and made XTOF measurements impossible. Samples **3** and **6** were not suitable for XTOF measurements because of high plasticity of their neat film. The injected carriers were found to distribute unevenly causing film deformation by electrostatic forces in the sites with high carrier density, and thus making carrier drift mobility unattainable. The continuous increase of μ_h with the applied electric field for all the DPA derivatives implies the governing role of energetic disorder[53] in the charge carrier transport of the wet-casted amorphous films. The high drift mobilities obtained for the nonsymmetric DPA derivatives **1**, **2**, **4**, **5** are well above usually reported values estimated in other DPA compounds.[26,27] Though remarkably high μ_h values (up to 10^{-2} cm^2/Vs) have also been achieved by introducing electron donating 9,10-arylamino units into the anthracene core.[29] However, the arylamino substitution enlarged conjugation of the DPA compound resulting in undesirable shift of the emission color to longer wavelengths (>450 nm).

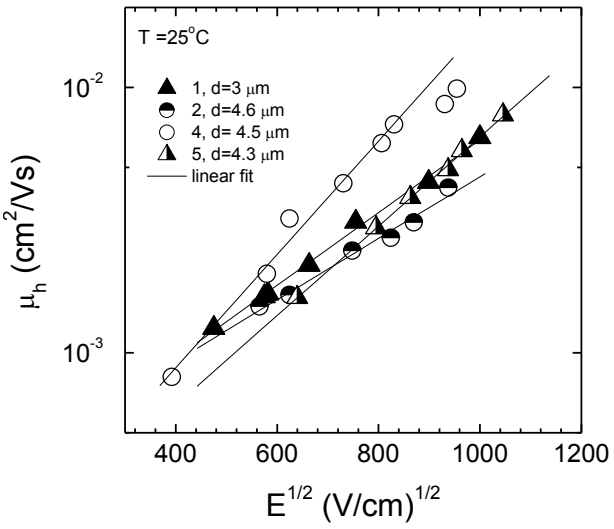

Figure 10. Hole drift mobility as a function of the applied electric field in the neat films of the DPA compounds **1**-**6**. Lines are guides for the eye. The average film thickness is indicated.

Ionization potentials (I_p) of the DPA derivatives **1**-**6** showed very similar values 5.74 - 5.9 eV comparable to those reported for 2-phenyl-substituted anthracene.[39]

Table 6. Hole drift mobilities and ionization potentials of the amorphous neat films of DPA derivatives **1**-**6**.

Compd.	μ_h (cm^2/Vs) @1 MV/cm [a]	I_p (eV) [b]
1	$4.6 \cdot 10^{-3}$	5.82
2	$6.5 \cdot 10^{-3}$	5.74
3	-	5.77
4	$9.9 \cdot 10^{-3}$	5.9
5	$6.5 \cdot 10^{-3}$	5.83
6	-	5.81

[a] Hole drift mobility of ambient atmosphere processed neat films.
[b] Ionization potential of ambient atmosphere processed neat films.

Conclusions

Realization of anthracene-based deep-blue emitters exhibiting fluorescence efficiency close to that of 9,10-diphenylanthracene (DPA), though, in the contrast to DPA, demonstrating good film forming properties and high carrier drift mobilities was attempted. To this end, a series of structurally modified nonsymmetric DPA derivatives with the phenyl and pentyl moieties at the 2nd position and the alkyl groups at the 9,10-phenyls were synthesized and investigated. Relatively small and poorly conjugated phenyl and pentyl substituents enabled to improve film forming properties by resulting in glass transition temperatures of up to 92 °C (for 2-phenyl moiety), meanwhile only up to -1 °C (for 2-pentyl moiety). The poorly conjugated 2-phenyl and 2-phentyl substituents weakly impacted transition energy in respect to the unsubstituted DPA resulting in the deep-blue emission with emission maxima below 450 nm. Absorption and fluorescence measurements supported by DFT calculations revealed relatively small shifts in singlet and triplet transition energies (<100 meV), which however, caused drastic changes in the intersystem crossing rate. Fluorescence measurements in dilute solution and rigid polymer matrix enabled to distinguish between the two possible pathways of nonradiative recombination, i.e. intramolecular torsions and intersystem crossing, and demonstrated the dominant role of the latter process. Roughly 10-fold and 5-fold increase in the intersystem crossing rate was obtained in the 2-phenyl- and 2-pentyl-substituted DPA compounds, respectively. Despite the large enhancement of the intersystem crossing rate the DPA compounds showed relatively high fluorescence quantum yields, up to 0.7 in a solution and up to 0.9 in a polymer host. The DPA derivatives exhibited almost no concentration quenching of fluorescence up to 8 wt % in PS matrix. Substitution at the 2nd position by pentyl moiety resulted in less pronounced concentration quenching as compared to the substitution by 2-phenyl group and also in respect to the unsubstituted DPA. The influence of the alkyl groups attached at the *para* position of 9,10-phenyls on the optical properties was found to be insignificant, whereas they strongly affected film forming and charge transport properties. It is worth noting that the nonsymmetric DPA derivatives expressed very high hole drift mobilities of up to $4.6 \cdot 10^{-3}$ cm^2/Vs for 2-phenyl-substituted compounds and up to almost $1 \cdot 10^{-2}$ cm^2/Vs for 2-pentyl-substituted analogues at an electric field of 1 MV/cm.
Further optimization of the DPA at the 2nd position by introducing nonconjugated and more branched or bulky substituents will enable to achieve even higher glass transition temperature and carrier drift mobility while preserving high fluorescence efficiency.

Acknowledgment

The research was funded by a grant (No. 31V-28) from the Science, Innovation and Technology Agency. The public access supercomputer from the High Performance Computing Center (HPCC) of the Lithuanian National Center of Physical and Technology Sciences (NCPTS) at Physics Faculty of Vilnius University (HPC Saulėtekis) was used for DFT calculations.

References

1. H. D. Becker, *Chem. Rev.*, 1993, **93**, 145–172.
2. M. Agbandje, T. C. Jenkins, R. McKenna, A. P. Reszka, and S. Neidle, *J. Med. Chem.*, 1992, **35**, 1418–1429.
3. S. Miyata, *Organic Electroluminescent Materials and Devices*, CRC Press, Florida, 1997.
4. Y. Inoue, S. Tokito, K. Ito, and T. Suzuki, *J. Appl. Phys.*, 2004, **95**, 5795–5799.
5. H. Meng, F. P. Sun, M. B. Goldfinger, G. D. Jaycox, Z. G. Li, W. J. Marshall, and G. S. Blackman, *J. Am. Chem. Soc.*, 2005, **127**, 2406–2407.
6. D. S. Chung, J. W. Park, J.-H. Park, D. Moon, G. H. Kim, H.-S. Lee, D. H. Lee, H.-K. Shim, S.-K. Kwon, and C. E. Park, *J. Mater. Chem.*, 2010, **20**, 524–530.
7. L. Valentini, D. Bagnis, A. Marrocchi, M. Seri, A. Taticchi, and J. M. Kenny, *Chem. Mater.*, 2008, **20**, 32–34.
8. C. Teng, X. Yang, C. Yang, S. Li, M. Cheng, A. Hagfeldt, and L. Sun, *J. Phys. Chem. C*, 2010, **114**, 9101–9110.
9. J. Shi and C. W. Tang, *Appl. Phys. Lett.*, 2002, **80**, 3201.
10. R. Kim, S. Lee, K.-H. Kim, Y.-J. Lee, S.-K. Kwon, J.-J. Kim, and Y.-H. Kim, *Chem. Commun.*, 2013, **49**, 4664.
11. S.-K. Kim, B. Yang, Y. Ma, J.-H. Lee, and J.-W. Park, *J. Mater. Chem.*, 2008, **18**, 3376.
12. D. Y. Kondakov, *J. Appl. Phys.*, 2007, **102**, 114504.
13. H. Fukagawa, T. Shimizu, N. Ohbe, S. Tokito, K. Tokumaru, and H. Fujikake, *Org. Electron.*, 2012, **13**, 1197–1203.
14. C.-J. Chiang, A. Kimyonok, M. K. Etherington, G. C. Griffiths, V. Jankus, F. Turksoy, and A. P. Monkman, *Adv. Funct. Mater.*, 2013, **23**, 739–746.
15. K. Nasu, T. Nakagawa, H. Nomura, C.-J. Lin, C.-H. Cheng, M.-R. Tseng, T. Yasuda, and C. Adachi, *Chem. Commun.*, 2013, **49**, 10385–10387.
16. S. S. Babu, M. J. Hollamby, J. Aimi, H. Ozawa, A. Saeki, S. Seki, K. Kobayashi, K. Hagiwara, M. Yoshizawa, H. Mohwald and T. Nakanishi, Nat. Commun., 2013, 4, 1969.
17. S. H. Lee, J. R. Lott, Y. C. Simon and Ch. Weder, J. Mat. Chem. C, 2013, 1, 5142.
18. P. Duan, N Yanai and N. Kimizuka, J Am Chem Soc, 2013, 135, 19056-19059
19. I. Cho, S. H. Kim, J. H. Kim, S. Park, and S. Y. Park, *J. Mater. Chem.*, 2012, **22**, 123–129.
20. B. Valeur, *Molecular fluorescence: principles and applications*, Wiley-VCH, Weinheim ; New York, 2002.
21. N. Nijegorodov, P. V. C. Luhanga, J. S. Nkoma, and D. P. Winkoun, *Spectrochim. Acta. A. Mol. Biomol. Spectrosc.*, 2006, **64**, 1–5.
22. J. V. Morris, M. A. Mahaney, and J. R. Huber, *J Phys Chem*, 1976, **80**, 969–974.
23. C. Adachi, T. Tsutsui, and S. Saito, *Appl. Phys. Lett.*, 1990, **56**, 799.
24. J.-K. Bin and J.-I. Hong, *Org. Electron.*, 2011, **12**, 802–808.
25. W. J. Jo, K.-H. Kim, H. C. No, D.-Y. Shin, S.-J. Oh, J.-H. Son, Y.-H. Kim, Y.-K. Cho, Q.-H. Zhao, K.-H. Lee, H.-Y. Oh, and S.-K. Kwon, *Synth. Met.*, 2009, **159**, 1359–1364.
26. S. C. Tse, S. K. So, M. Y. Yeung, C. F. Lo, S. W. Wen, and C. H. Chen, *Chem. Phys. Lett.*, 2006, **422**, 354–357.
27. M.-H. Ho, Y.-S. Wu, S.-W. Wen, M.-T. Lee, T.-M. Chen, C. H. Chen, K.-C. Kwok, S.-K. So, K.-T. Yeung, Y.-K. Cheng, and Z.-Q. Gao, *Appl. Phys. Lett.*, 2006, **89**, 252903.
28. M.-H. Ho, B. Balaganesan, and C. H. F. Chen, *Isr. J. Chem.*, 2012, **52**, 484–495.

29. Y.-J. Pu, A. Kamiya, K. Nakayama, and J. Kido, *Org. Electron.*, 2010, **11**, 479–485.
30. Y. Sun, L. Duan, D. Zhang, J. Qiao, G. Dong, L. Wang, and Y. Qiu, *Adv. Funct. Mater.*, 2011, **21**, 1881–1886.
31. J. C. de Mello, H. F. Wittmann, and R. H. Friend, *Adv. Mater.*, 1997, **9**, 230–232.
32. P. M. Borsenberger, *Organic photoreceptors for xerography*, Marcel Dekker, New York, 1998.
33. E. Montrimas., V. Gaidelis., and A. Pazera., *Lith. J. Phys.*, 1966, **6**, 569–418.
34. S. M. Vaezi-Nejad, *Int. J. Electron.*, 1987, **62**, 361–384.
35. V. Sivamurugan, R. Lygaits, J. V. Gražulevičius, V. Gaidelis, V. Jankauskas, and S. Valiyaveettil, *J. Mater. Chem.*, 2009, **19**, 4268.
36. M. Kirkus, R. Lygaitis, M.-H. Tsai, J. V. Grazulevicius, and C.-C. Wu, *Synth. Met.*, 2008, **158**, 226–232.
37. M. J. Frisch, G. W. Trucks, H. B Schlegel, G. E. Scuseria., M. A Robb et. al., *Gaussian 09*, Gaussian Inc;, Wallingford, CT, 2013.
38. A. V. Kukhta, I. N. Kukhta, N. A. Kukhta, O. L. Neyra, and E. Meza, *J. Phys. B At. Mol. Opt. Phys.*, 2008, **41**, 205701.
39. T. Serevičius, P. Adomėnas, O. Adomėnienė, R. Rimkus, V. Jankauskas, A. Gruodis, K. Kazlauskas, and S. Juršėnas, *Dyes Pigments*, 2013, **98**, 304–315.
40. I. B. Berlman, *Handbook of fluorescence spectra of aromatic molecules*, Academic Press, New York, 2d ed., 1971.
41. Z.-Q. Wang, C. Xu, W.-Z. Wang, L.-M. Duan, Z. Li, B.-T. Zhao, and B.-M. Ji, *New J. Chem.*, 2012, **36**, 662.
42. M.-G. Shin, S. O. Kim, H. T. Park, S. J. Park, H. S. Yu, Y.-H. Kim, and S.-K. Kwon, *Dyes Pigments*, 2012, **92**, 1075–1082.
43. R. E. Kellogg, *J. Chem. Phys.*, 1966, **44**, 411.
44. D. Oelkrug, A. Tompert, H. Egelhaaf, M. Hanack, E. Steinhuber, M. Hohloch, H. Meier, and U. Stalmach, *Synth. Met.*, 1996, **83**, 231–237.
45. K. Kazlauskas, A. Miasojedovas, D. Dobrovolskas, E. Arbačiauskienė, V. Getautis, A. Šačkus, and S. Juršėnas, *J. Nanoparticle Res.*, 2012, **14**, 877–890.
46. R. Kersting, B. Mollay, M. Rusch, J. Wenisch, G. Leising, and H. F. Kauffmann, *J. Chem. Phys.*, 1997, **106**, 2850.
47. R. Karpicz, S. Puzinas, S. Krotkus, K. Kazlauskas, S. Jursenas, J. V. Grazulevicius, S. Grigalevicius, and V. Gulbinas, *J. Chem. Phys.*, 2011, **134**, 204508.
48. K. N. Solov'ev and E. A. Borisevich, *Phys.-Uspekhi*, 2005, **48**, 231–253.
49. J. Qu, J. Zhang, A. C. Grimsdale, K. Müllen, F. Jaiser, X. Yang, and D. Neher, *Macromolecules*, 2004, **37**, 8297–8306.
50. J. C. Ribierre, A. Ruseckas, H. Cavaye, H. S. Barcena, P. L. Burn, and I. D. W. Samuel, *J. Phys. Chem. A*, 2011, **115**, 7401–7405.
51. A. Miasojedovas, K. Kazlauskas, G. Armonaite, V. Sivamurugan, S. Valiyaveettil, J. V. Grazulevicius, and S. Jursenas, *Dyes Pigments*, 2012, **92**, 1285–1291.
52. S. Krotkus, K. Kazlauskas, A. Miasojedovas, A. Gruodis, A. Tomkeviciene, J. V. Grazulevicius, and S. Jursenas, *J Phys Chem C*, 2012, **116**, 7561–7572.
53. H. Bässler, *Phys. Status Solidi B*, 1993, **175**, 15–56.

Table of contents

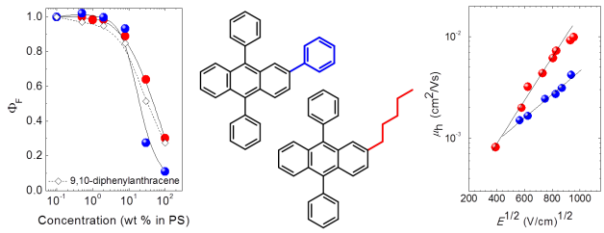

Realization of 9,10-diphenylanthracene based deep-blue emitters exhibiting high fluorescence efficiency, demonstrating good film forming properties and high carrier drift mobilities is presented.